Axial Morphology along the Southern Chile Rise

D.K. Blackman[a*], B. Appelgate[a], C.R. German[b], A.R. Thurber[a,c], A.S. Henig[a]

[a] *Scripps Institution of Oceanography, UCSD, La Jolla CA 92093 USA*

[b] *Woods Hole Oceanographic Institution, Woods Hole MA 02543 USA*

[c] *present address COAS, Oregon State University, OR 97331 USA*

[*] *corresponding author, dblackman@ucsd.edu 858-534-8813, 858-534-5332 fax*

Abstract

Morphology of four spreading segments on the southern Chile Rise is described based on multi-beam bathymetric data collected along the axial zones. The distribution of axial volcanoes, the character of rift valley scarps, and the average depths vary between Segment 1 in the south, terminating at the Chile Triple Junction, and Segment 4 in the north, which are separated by three intervening transform faults. Despite this general variability, there is a consistent pattern of clockwise rotation of the southern-most axial volcanic ridge within each of Segments 2, 3, and 4, relative to the overall trend of the rift valley. A combination of local ridge-transform intersection stresses and regional tectonics may influence spreading axis evolution in this sense.

Keywords.

Chile Rise; mid-ocean ridge; oceanic spreading center; axial morphology

1. Introduction

The Chile Rise extends south from the Valdivia fracture zone system as a series of spreading segments that increase in proximity to the Chile trench until the triple junction is reached. The intersecting segment is being overridden by the South American Plate (Figure 1), thus the Chile Triple Junction (CTJ) is the only place on earth where an actively spreading mid-ocean ridge is being subducted under a continental plate. This plate boundary geometry provides a natural laboratory for investigation of the interplay between surface tectonics and underlying mantle processes, specifically upwelling patterns and associated magma production that supplies new forces. Detailed morphologic patterns observed within the axial zone of the four southernmost

segments provide initial insights into some aspects of this interplay. Ridge subduction has occurred elsewhere in the past so results from the current Chile system can provide insight into evolution of ancient ridge-trench, and associated micro-plate, systems. With a half rate of 30 mm/yr (Cande et al., 1987), the Southern Chile Rise sits at a threshold, typical of intermediate spreading ridges, where a variety of factors can influence the axial structure (Baran et al., 2005, Martinez et al., 2006). This paper presents maps of new data, reports on the observed trends and character of the axial volcanoes and fault scarps, and discusses potential regional influences on the pattern. While the new coverage is modest, mostly a single bathymetric swath that just reaches the edge of the axial zone, it identifies persistent clockwise rotation trends in the southern ends of three successive segments. These new data allow us to begin to place the plate boundary evolution into a context of regional controlling forces.

The bathymetry data were obtained on two *R/V Melville* cruises (MV1003 and MV1016) in 2010. The first was part of a NOAA Ocean Exploration study (INSPIRE- Chile 2010; International Southeast Pacific Investigation of Reducing Environments) that emphasized water column plume mapping and seafloor sampling of biological specimens within seep and prospective hydrothermal vent areas. The bathymetric data provided context for these targeted studies. The second cruise represented opportunistic data acquisition during an equipment testing program. The INSPIRE- Chile 2010 cruise obtained essentially complete coverage of the axial zones of Segments 1 and 2, immediately north of the Chile Triple Junction (CTJ) at a resolution improved relative to prior data. Subsequently, almost complete coverage of the axial zones of Segments 3 and 4 was obtained, much of which is the first available ~100-m resolution data. Regional bathymetric data were available from prior cruises by Chilean, French, German and U.S. scientists (Cande et al., 1987, Bourgois et al., 2000).

The INSPIRE- Chile 2010 EM122 data, obtained at ~1.5 kt speeds during tow-yo runs, required modest ping editing prior to gridding (50 m spacing). These data (weight=1.0) were then combined with the regional grid values (100 m spacing, weight=0.25) and surface fit using GMT (Wessel and Smith, 1998) to produce a 50-m grid. Artifacts are evident along regional tracks but the axial regions are best illustrated with this choice of surface ‘tension’ and grid spacing. MV1016 data, collected at underway speeds, have not been edited significantly; these data were gridded at 100 m spacing.

2. Morphologic Observations

The axial morphology of the Chile Rise varies along the four segments extending north from the Chile Triple Junction- Segments 1 through 4, respectively. The general character of Segments 1 and 3 is similar to other intermediate spreading rate axial zones (Kappel and Ryan, 1986), with 5-8 km wide, fairly linear rift valley within which a 1-2 km wide volcanic zone occurs. As noted by previous workers (Klein and Karsten, 1995, Bourgois et al., 2000), Segment 2 is deeper than the adjacent segments, with average axial depth of almost 4000 m compared to 3200-3300 m depths along Segments 1 and 3. Segment 4 comprises a series of elongate sub-basins slightly offset from one another along the overall rift trend. Axial depths for Segment 4 range from ~4000 m in the sub-basins, through an average of ~3650 m, to a shoal section of ~2750 m near the southern end. Below we describe the morphology of the axial zone along each segment, from south to north.

Segment 1 is 50 km long and the depth of the rift valley floor is consistently ~3200 m to the north of where slope sediments begin to fill the central graben (~46°05'S, Figure 2a). The pre-existing EM12 bathymetry data (Bourgois et al., 2000) showed the main morphology of this segment and those authors adopted the termination of high-backscatter volcanic structures against the scarp at the toe of the slope at 46°09'S as the precise location of the triple junction. Our higher resolution (narrower sonar beam) coverage shows additional detail within the rift axis and we include the section that continues to be bounded by small western rift wall fault scarps in our defined segment length, which extends south to ~46°16'S. A chain of volcanic structures <400 m in diameter tracks the central graben in the northern half of the segment (Figure 2a). From 46°06'-46°12'S, several axial seamounts with diameter ~1 km are evident above the sediment fill, most located on a likely fault-controlled shelf on the slope side of the spreading axis, but a few occur near or just west of the center of the rift. There is a deviation in axial linearity evident on the western valley wall between ~46°08' and 46°11'S, where scarps strike several degrees west of the main axial trend. Axial volcanoes within this section are distributed more widely across the median valley but do not clearly line up with the deviated scarp trend. Western valley wall scarps along the southern, unsubducted portion of the axial valley 46°12-16'S resume the main trend of the segment. Fault scarps extend linearly for 12-15 km distances throughout the segment and have throws of 50-75 m within the rift valley floor.

93 Segment 2, which is offset about 50 km west along the Darwin transform fault, is
94 characterized by an almost 1 km deep rift valley (Figure 2b). The nodal basins at the ends of this
95 43 km long segment are more than 4000 m deep and the central portion of the segment has axial
96 depths ~3800 m. Small, linear volcanic chains occur along most of the axis but their location
97 within the rift valley varies along strike (Figure 2b). As the volcanic features rise above the nodal
98 basin in the north, they are centered within the main rift valley. In the central part of the segment,
99 the volcanic chain hugs the eastern scarp of the rift. In the south half of the segment, the chain
100 has crossed the axis and tracks along the western edge of the rift valley floor before activity
101 apparently tapers off ~45°56'S. In the southern half of the segment, the axial volcanoes trend
102 about 16° clockwise from the average trend of the rift valley, projecting obliquely into the
103 Darwin fracture zone.
104 Segment 3 is the most linear of the southern Chile Rise segments studied; it extends 152 km
105 and has two clear deviations in axial linearity (45°20'S and ~45°05'S, Figure 3a). Linear scarps
106 are sub-parallel throughout the segment though individual sections often curve slightly near their
107 terminations. Contiguous scarp lengths are 5-15 km with corresponding throws of 75~400 m.
108 Distinct volcanic cones in the southern end of Segment 3 (Figure 2c) are generally small (350-
109 500 m diameter, <75 m high). A rifted linear high makes up the axial zone in the section from
110 45°25' to 45°40'S. Volcanic cones are sparse in this area but increase in number and continuity
111 as the rifted high transitions to a graben approaching the Guamblin transform fault to the South.
112 Similar to Segment 2, the volcanic features associated with this apparent recent activity in the
113 southern end of the segment trend 8° clockwise from the overall (end-to-end) trend of Segment
114 3. An increase in the size of the conical axial volcanoes, to diameter ~1 km, and a tendency for
115 them to be flat-topped, occurs throughout the northern part of Segment 3 (top of Figure 2c,
116 where the pattern begins and continues northward, Figure 3a). Spacing between these features is
117 2-4 km in the central and northern portions of the segment. The interval 45°10'- 44°40'S has
118 more continuous small (likely volcanic) axial ridges and adjacent narrow grabens, with just a few
119 distinct volcanic cones, 125-200 m high with diameter 1-2 km. The relief dropping into the axial
120 rift is 500-700 m for much of the northern half of the segment. The axial high in the southern
121 part of the segment has relief of 200-300 m, relative to the adjacent flanks.
122 The new multi-beam coverage along Segment 4 is not quite wide enough to fully capture the
123 axial zone and bounding rift walls but several aspects of the morphology can be described in

significantly greater detail than was possible previously. In contrast to the relative continuity of Segment 3, Segment 4 comprises a series of 20-30 km long sections of varied morphology (Figure 3b) within the 228 km total length. The southernmost and central sections have ~5 km wide axial valleys with 200-300 m high axial volcanic ridges running down the middle. A shallow section occurs at the southern end of this segment, ~20 km north of the Guafo transform fault (Figure 2d). Beyond that (44°25' - 43°40'S), the axis is characterized by an elongate basin with hummocky floor and a few flat-topped volcanoes; this section has a steeper rift-valley wall on the east than on the west. The northern third of the segment (Figure 3b) has numerous axial volcanic cones and modest scarps (50-100 m high) but neither type of feature is continuous or localized within the axial zone covered. Moderate-sized, flat-topped axial volcanoes are common and can be seen extending all the way to the southern intersection of Segment 4 with the Guafo transform fault. As seen in Segments 2 and 3, the trend of this southern-most axial volcanic ridge and that of a distinct scarp to its west (Figure 2d) are rotated 10° clockwise relative to the main trend of the full Segment 4.

3. Discussion

There is a consistent pattern of the axial volcanic ridges in the southern part of the (non-subducting) segments in our study area trending at an angle that is rotated several degrees clockwise from the overall trend of the rift valley. Clearly the eruptive centers are taking advantage of a zone of weakness that currently has this rotated alignment near the south-bounding transform faults, but whether the underlying melt supply has also recently shifted is not known. At the southern Segment 2 ridge-transform intersection (RTI), it is intriguing that the nodal deep, which is often modeled as the result of viscous mantle flow and plate stresses at a RTI (Sleep and Biehler, 1970, Parmentier and Forsyth, 1985, Blackman, 1997), is centered on the opposite (east) side of the rift valley from the axial volcanic ridge on the western side. This may indicate that mantle upwelling is centered in the east, despite apparent recent magmatic activity having occurred on the other side of the rift. Presumably this apparently contradictory morphology reflects interplay between local magma plumbing and tectonic stresses. In addition to the RTI related forces, regional factors associated with subduction of the Nazca plate may affect mantle flow, melting, and detailed kinematics; the results for Segments 3 and 4 suggest this could be the case, as we discuss below.

Interpretation of clockwise stress rotation within the corridor containing Segment 2 has previously been reported (Villanueva et al., 1997). These investigators documented flank deformation patterns and magnetic anomalies out to 1.5 Ma crust. They note an associated decrease to 30 mm/yr in half-spreading rate along this segment, whereas their analysis suggested the adjacent segments continued at a half-rate of 33 mm/yr since 1.5 Ma.

Various CTJ investigators have identified three factors in the overall tectonic system that could contribute to along-strike variation in far field forces which might impact the stress field along the Chile Rise as it extends north: 1) increase in age of the subducting Nazca plate north from CTJ (Cande et al., 1987) which could correspond to reduced slab buoyancy in the north; 2) the small volume of the accretionary wedge near CTJ and subduction erosion there, versus the occurrence of down-going sediments (and fluids) between Taitao FZ and Tres Montes FZ, to the south of CTJ, which may ease descent of the slab along the latter section (Behrmann and Kopf, 2001); 3) variation in dip and continuity (slab tears) of the down-going plate, outer-rise flexure, and associated westward ridge jumps toward new zones of weakness (Bourgois et al., 2000, Guivel et al., 2003, Breitsprecher and Thorkelson, 2009). Below, we discuss the sense of rotation that each of these factors would induce along the Chile Rise and whether that could explain why the southernmost part of the segments is most strongly affected.

Lagabrielle and coworkers have done considerable work onshore that documents opening of a slab window and associated petrological and structural impacts in the obducted ophiolites around Taitao Peninsula (Forsythe et al., 1986; Lagabrielle et al., 1994; Guivel et al., 2003). As part of Bourgois et al. (2000)'s offshore study, Lagabrielle's group focused on the evolution of Segment 2, its bounding fracture zones, and the adjacent flanks of Segments 1 and 3 (Villanueva et al., 1997, Lagabrielle pers. comm. 2011). These authors analyzed morphology, backscatter, and magnetic anomaly patterns to develop a model where observed seafloor deformation and evolution from an axial high to segmented rift is associated with the approach of Segment 1 to the trench. Thus, their preferred explanation for spreading center evolution and fracture zone sinuosity is plate edge-dominated tectonic forces. Resistance to subduction of the active spreading center acts to anchor the SE part of the plate whereas it can continue to subduct to the north. This scenario could be expected to result in clockwise rotation of stress but would not, alone, predict the effect to be most prominent in the southern part of each spreading segment.

A northward increase in subduction pull associated with greater downgoing plate age might be expected to result in monotonically increasing extensional forces to the north. Tebbens et al. (1997), however, determine that recent spreading rates along the southern Chile Rise varied by only 0.6 mm/yr. Even with such modest variation, if the thickness of the plate edge across each of the southern RTIs of Segments 2-4 acts to anchor the corner of the eastern flank there, then a clockwise rotation of stress could result. However, this regional force should also be evident in the northern part of the segments, perhaps as greater rift depths, if magma supply is fairly constant along axis. This type of pattern is not observed. Perhaps the variable along-strike sediment accretion/deformation plays a role in counter-acting any plate age effects. Behrmann and Kopf (2001) determined that sediment accretion and deformation are greater on the flank of Segment 3 than along the flank of Segment 1, where sediments and associated fluids are being subducted.

In addition to the potential plate edge effects, spreading center structure and processes need to be considered. There has been a decrease in spreading rate, from ~60 mm/yr (full rate) in the chron 2A-Jaramillo period to ~53 mm/yr presently (DeMets et al., 2010). This crosses the threshold where prior studies indicate that shorter segment length is preferred over long, continuous segments (e.g. Crane, 1985; Schouten et al., 1985). In the South Atlantic, average segment length decreased significantly as the spreading center slowed from a rate of 60 mm/yr to ~30 mm/yr over a period of a few Myr (Cande et al., 1988; Shaw and Cande, 1990). Although such segmentation of the volcanic system would not explain a systematic rotation, it could affect the continuity of volcanic chains. Segment 2 axial volcanoes could be described as a series of offset short chains (Lagabrielle pers. comm. 2011) with both a central and southern chain having the rotation indicated in Figure 2b and a series of small step-overs near 45°50'S. Segment 4 axial structure may be best described as a series of short rift/volcanic systems but such a description is not applicable to Segment 3. Magma supply at the latter has probably been greater recently, as evidenced by the axial high that characterizes the southern section of its spreading axis, seamounts on the adjacent western ridge flank (Figure 1; Klein and Kastens, 1995), and documented mantle source heterogeneity there (Sturm et al., 1999). Each of these indicates a melting anomaly. Reduction of axial stress would be expected to accompany more frequent magmatic injection and probably played a role in the greater continuity of the structural fabric of

Segment 3, compared with Segments 2 and 4, whose greater axial depth suggests lower magma supply.

Another potential factor in the evolution of stress along the spreading axes is the recent intersection of Segment 1 with the trench at ~0.3 Ma (Bourgois et al., 2000). Does such change from previously younging (thinning and weaker, in the up-trench direction) lithosphere entering the trench to an increasing age/thickness (west flank) lithosphere alter the forces on the Nazca plate as it enters the trench to affect the next segment's spreading axis? Or, is the buoyancy of the zero-age axial region so great that a pause in subduction occurs near the triple junction, thus altering the axial stress field at adjacent segments? The fact that Segment 1 does not appear to have experienced any rotation in axial trend does support a model where the ridge-trench collision plays a role. If subduction begins to hang up near the triple junction for a period shortly after the axis of spreading intersects the trench (i.e. it takes some time for the finite width structure to be over-ridden enough that the new set of forces becomes dominant), this, together with steps in plate thickness across fracture zones to the north, could put the Nazca and Pacific plates under compression that has a major component in the N-S direction, the sense needed to cause the observed axial rotation. There are clearly responses along other parts of the plate boundary to the collision. For example, an area of chaotic terrain has developed along the short-offset, short segments just south of Valdivia transform fault (41°30'-42°10'S, ~84°W; evident using GeoMapApp and multi-beam data in the Marine Geosciences Data System (MGDS), (Ryan et al., 2009)). These features suggest notable realignment, and possible propagation in crust that formed ~350 Ka, i.e. essentially synchronous with when the southern end of Segment 1 first reached the trench. More complete coverage of Segment 4 is needed to determine whether such features developed south of 42°S, but the current coverage suggests that linear abyssal hills are most typical for longer segments (north of Chiloe (MGDS, (Ryan et al., 2009)), and Segments 4 & 3, in the southward direction, Figure 1) at this time.

Constraints on mantle structure and possible flow pattern are available from a recent seismic array experiment. Russo et al. (2010) obtained tomographic images that show a fast anomaly (cold slab) to the north of Taitao Peninsula but only a slow anomaly to the south, where a slab window had been expected. Shear wave splitting results show a somewhat complex pattern of fast S-wave polarization directions, which are inferred to track the path of mantle shearing, that is generally consistent with flow along the trench and in through the slab window. Such broad

scale flow has potential to skew upwelling patterns for Segment 1 and, possibly, Segment 2. However, a southward along-trench flow would not tend to shift the upwelling/melting to the west, nor would it favor such direction mainly toward the south.

Klein and co-workers conducted a study of axial basalts along the southern Chile Rise. Their major element analyses (Klein and Karsten, 1995, Sherman et al., 1997) show that the lavas are mid-ocean ridge basalt (MORB) with varying parental compositions and degrees of fractionation. Extents and initial pressures of melting were found to be generally similar for Segments 1-4 and, thus, Sherman et al. (1997) conclude that proximity to the trench, and even the onset of ridge subduction, do not significantly modify major element systematics. They infer that this indicates that the upwelling zone beneath the spreading axis is narrow. The observed distinct trace element and isotopic signatures for each of Segments 1-4 (Klein and Karsten, 1995, Sherman et al., 1997, Sturm et al., 1999) suggest a model where mantle flow pattern exerts at least some control over detailed location of the spreading axis. A transform fault effect has been ruled out as the cause of petrological differences across segment boundaries (Sherman et al., 1997). However, there is no clear reason why pre-existing tectonic boundaries would 'seek out' chemical boundaries in the mantle over which to advance, so at this time we prefer an interpretation where subducting plate-edge forces are the dominant control on the spreading axis evolution.

4. Conclusions

New mapping of the axial zones of the southern Chile Rise shows several degree rotation of the recent stress field that controls the trend of volcanic eruptions in the southern portion of Segments 2-4. Simple models of ridge-transform intersection forces do not explain this recent evolution in trend. Regional tectonic forces probably influence the plate boundary evolution, but the lack of monotonic change with distance from the CTJ suggests that a single factor is not responsible. Likely, some combination of plate edge forces, such as age-dependent lithosphere buoyancy and resistance to subduction due to sediment scrape off and/or the intersection of Segment 1 spreading axis with the trench, are in play.

Acknowledgements. We thank the Melville captain and crew for their support during the data acquisition. Steve Cande pointed out the association between recent plate spreading rate

changes and the morphology of the youngest crust in areas north of Segment 4. This work was supported by NOAA/OE grant NA08OAR4600757 and University of California Ship Funds.

References

Baran, J.M., J. R. Cochran, S. M. Carbotte, Nedimovic´, M.R., 2005. Variations in upper crustal structure due to variable mantle temperature along the Southeast Indian Ridge. Geochemistry Geophysics Geosystems 6**,** Q11002.

Behrmann, J., Kopf, A., 2001. Balance of tectonically accreted and subducted sediment at the Chile Triple Junction, International Journal Earth Science (Geol Rundsch) 90**,** 753-768.

Blackman, D.K., 1997. Variation in lithospheric stress along ridge-transform plate boundaries. Geophysical Research Letters 24**,** 461-464.

Bourgois, J., C Guivel, Y Lagabrielle, T Calmus, J Boulégue, Daux, V., 2000. Glacial-interglacial trench supply variation, spreading ridge subduction, and feedback controls on the Andean margin development at the Chile triple junction area (45-48°S). Journal of Geophysical Research B 105**,** 8355-8386.

Breitsprecher, K., Thorkelson, D.J., 2009. Neogene kinematic history of Nazca-Antarctic-Phoenix slab windows beneath Patagonia and the Antarctic Peninsula. Tectonophysics 464**,** 10-20.

Cande, S., RB Leslie, JC Parra, Hobart, M., 1987. Interaction between the Chile Rise and Chile Trench: geophysical and geothermal evidence. Journal of Geophysical Research B 92**,** 495-520.

Cande, S.C., LaBrecque, J.L., Haxby, W.F., 1988. Plate kinematics of the south Atlantic: chron C34 to present. Journal of Geophysical Research B 93**,** 13,479-413,492.

Crane, K., 1985. The spacing of ridge axis highs: dependence upon diapiric processes in the underlying asthenosphere? Earth and Planetary Science Letters 72**,** 405-414.

DeMets, C., Gordon, R.G., Argus, D.F., 2010. Geologically current plate motions. Geophysical Journal International 181, 1–80.

Forsythe, R. D., Nelson, E. P., Carr, M. J., Kaeding, M. E., Hervé, M., Mpodozis, C. M., Soffia, M. J., Harambour, S., 1986. Pliocene near trench magmatism in southern Chile : A possible manifestation of ridge collision. Geology 14, 23-27.

307 Guivel, C., Y Lagabrielle, J Bourgois, H Martin, N Amaud, S Fourcade, J Cotten, Maury, R.,
308 2003. Very shallow melting of oceanic crust during spreading ridge subduction: Origin of
309 near-trench Quaternary volcanism at the Chile Triple Junction. Journal of Geophysical
310 Research B 108, 2345.
311 Kappel, E.S., Ryan, W.B.F., 1986. Volcanic Episodicity and a Non-Steady State Rift Valley
312 Along Northeast Pacific Spreading Centers: Evidence From Sea MARC I. Journal of
313 Geophysical Research B 91**,** 13,925–13,940.
314 Klein, E.M., Karsten, J.L., 1995. Ocean ridge basalts with convergent margin geochemical
315 affinities from the Chile Ridge. Nature 374**,** 52-57.
316 Lagabrielle Y., Le Moigne J., Maury R.C., Cotten J., Bourgois J., 1994. Volcanic record of the
317 subduction of an active spreading ridge, Taitao Peninsula (southern Chile). Geology 22,
318 515-518.
319 Martinez, F., Taylor, B., Baker, E.T., Resing, J.A., Walker, S.L., 2006. Opposing trends in
320 crustal thickness and spreading rate along the back-arc eastern Lau spreading center:
321 implications for controls on ridge morphology, faulting, and hydrothermal activity. Earth
322 and Planetary Science Letters 245**,** 655–672.
323 Parmentier, E.M., Forsyth, D.W., 1985. Three-dimensinoal flow beneath a slow-spreading ridge
324 axis: a dynamic contribution to the deepening of the median valley toward fracture zones.
325 Journal of Geophysical Research B 90**,** 678-684.
326 Russo, R., J.C. VanDecar, D. Comte, V.I .Mocanu, A. Gallego, Murdie, R., 2010. Subduction of
327 the Chile Ridge: Upper mantle structure and flow. Geological Society of America Today
328 20**,** 4-10.
329 Ryan, W.B.F., S.M. Carbotte, J. Coplan, S. O'Hara, A. Melkonian, R. Arko, R.A. Weissel, V.
330 Ferrini, A. Goodwillie, F. Nitsche, J. Bonczkowski, Zemsky, R., 2009. Global Multi-
331 Resolution Topography (GMRT) synthesis data set. Geochemistry Geophysics
332 Geosystems 10**,** Q03014.
333 Schouten, H., K.D. Klitgord, Whitehead, J.A., 1985. Segmentation of mid-ocean ridges. Nature
334 317**,** 225-229.
335 Shaw, P.R., Cande, S.C., 1990. High resolution inversion for South Atlantic plate kinematics
336 using joint altimeter and magnetic anomaly data. Journal of Geophysical Research B 95**,**
337 2625-2644.

338 Sherman, S.B., J.L. Karsten, Klein, E.M., 1997. Petrogenesis of axial lavas from the southern
339 Chile Ridge: major element constraints. Journal of Geophysical Research B 102**,** 14,963-
340 14,990.
341 Sleep, N.H., Biehler, S., 1970. Topography and tectonics at the intersection of fracture zones
342 with central rifts. Journal of Geophysical Research, B 75**,** 2748-2752.
343 Smith, W.H.F., Sandwell, D.T., 1997. Global seafloor topography from satellite altimetry and
344 ship depth soundings. Science 277, 1956-1962.
345 Sturm, M.E., E.M. Klein, D.W. Graham, Karsten, J., 1999. Age constraints on crustal recycling
346 to the mantle beneath the southern Chile Ridge: He-Pb-Sr-Nd isotope systematics.
347 Journal of Geophysical Research B 104**,** 5097-5114.
348 Tebbens, S.F., S.C. Cande, L. Kovacs, J.C. Parra, J.L. LaBrecque, Vergara, H., 1997. The Chile
349 Ridge: A tectonic framework. Journal of Geophysical Research B 102**,** 12,035-012,059.
350 Villanueva, G., M. Ravilly, J. Bourgois, Y. Lagabrielle, Dyment, J., 1997. Seaward propagation
351 of ridge-subduction induced deformation (Chile Triple Junction area): Bathymetric and
352 magnetic evidences. Eos Transactions AGU 78 Fall Mtg Suppl.**,** 674.
353 Wessel, P., Smith, W.H.F., 1998. New, improved version of the Generic Mapping Tools. Eos
354 Transactions AGU 79**,** 579.

Figure Captions

Figure 1. Bathymetry along the Southern Chile Rise shows spreading segments and fracture zones; illumination angle NNE. Inset shows main tectonic elements: VFZ- Valdivia Fracture Zone; CTJ- Chile Triple Junction. Segment 1 terminates in the south at the CTJ. New multibeam bathymetry data along the ridge axes are overlain on regional grid (compilation of German, French, and Chilean data by I. Grevemeyer, incorporates partial flank coverage of Segments 1-3), and satellite-based predicted bathymetry (Smith and Sandwell, 1997).

Figure 2. Detailed axial morphology shows differences between average segment trend and trend of recent volcanic or fault scarp features. Each of Segments 2, 3, and 4 show recent trends in the south (red arrows) that are 16°, 8°, & 10° clockwise from the average (black arrows). Illumination angle NE.

Figure 3. Bathymetry of the full length of Segment 3 (left) and Segment 4 (right); color scale the same as in Fig. 2.

Figure 1

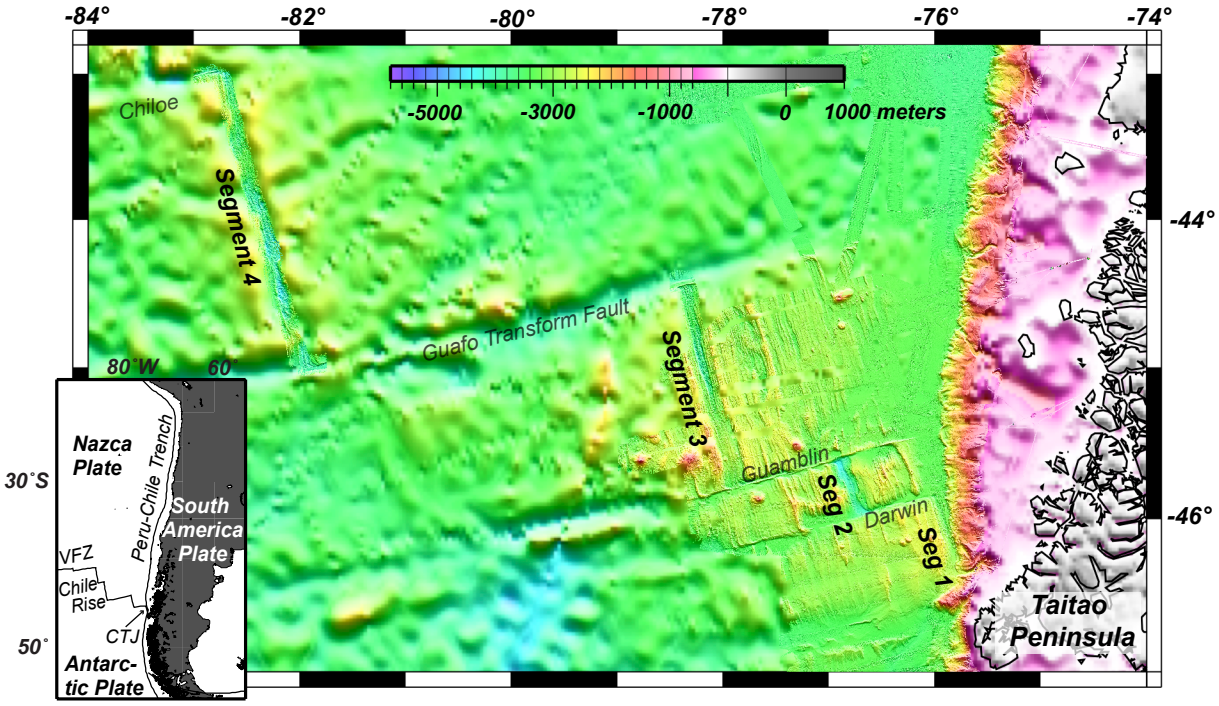
-84°
-82°
-80°
-78°
-76°
-74°
-44°
-46°
-5000
-3000
-1000
0
1000 meters
Chiloe
Segment 4
Guafo Transform Fault
Segment 3
Guamblin
Seg 2
Darwin
Seg 1
Taitao Peninsula
80°W
60
30°S
50°
Nazca Plate
Peru-Chile Trench
South America Plate
VFZ
Chile Rise
CTJ
Antarc-tic Plate

Figure 2

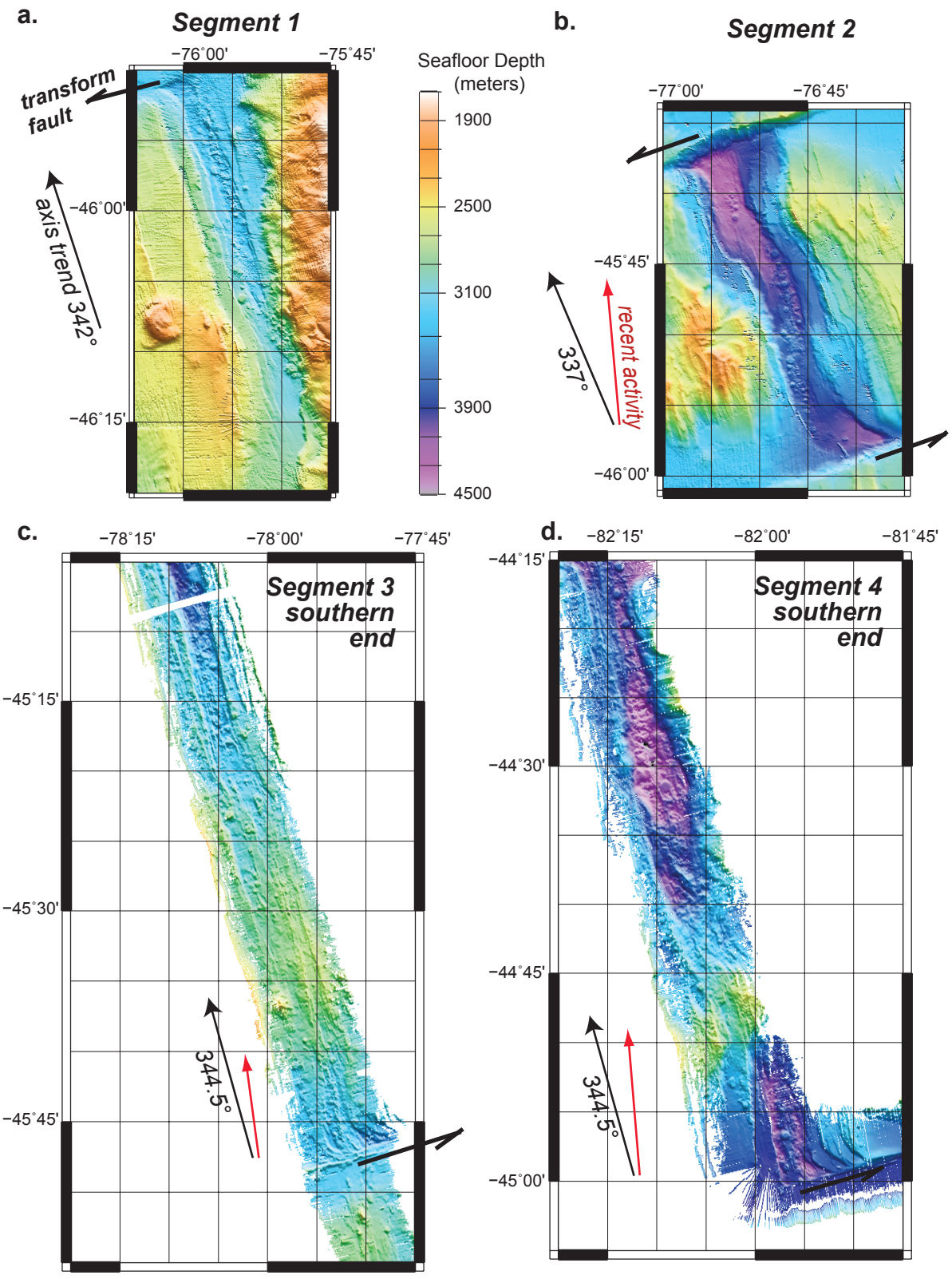
a.
Segment 1
−76˚00'
−75˚45'
transform fault
axis trend 342°
−46˚00'
−46˚15'
Seafloor Depth (meters)
1900
2500
3100
3900
4500
b.
Segment 2
−77˚00'
−76˚45'
−45˚45'
recent activity
337°
−46˚00'
c.
−78˚15'
−78˚00'
−77˚45'
Segment 3 southern end
−45˚15'
−45˚30'
344.5°
−45˚45'
d.
−82˚15'
−82˚00'
−81˚45'
−44˚15'
Segment 4 southern end
−44˚30'
−44˚45'
344.5°
−45˚00'

Figure 3

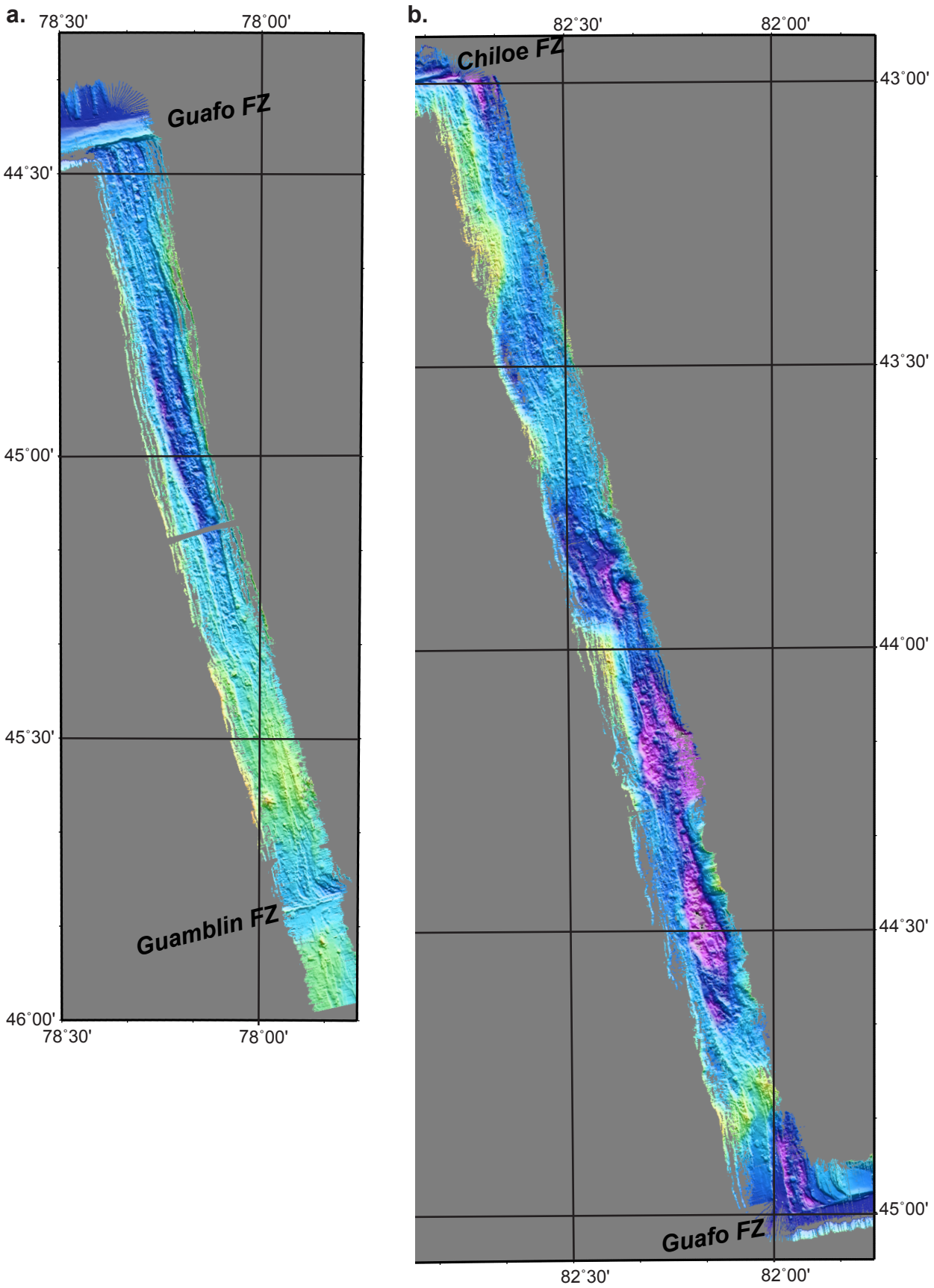
a.
78°30'
78°00'
Guafo FZ
44°30'
45°00'
45°30'
Guamblin FZ
46°00'
78°30'
78°00'
b.
82°30'
82°00'
Chiloe FZ
43°00'
43°30'
44°00'
44°30'
45°00'
Guafo FZ
82°30'
82°00'